Geophysical Research Letters

RESEARCH LETTER
10.1029/2019GL086736

Key Points:
- Historic U.S. heat waves are investigated in high-resolution WRF simulations nudged toward reanalysis with and without anthropogenic warming
- Dry heat waves become drier, and humid heat waves stay humid in a warmer climate, showing temperature-driven increase in future heat stress
- Results suggest thermodynamic drivers dominate future changes in characteristics of both dry and humid heat waves

Supporting Information:
- Supporting Information S1
- Figure S1
- Figure S2
- Figure S3
- Figure S4
- Figure S5
- Figure S6
- Figure S7
- Figure S8
- Figure S9

Correspondence to:
D. Rastogi,
rastogid@ornl.gov

Citation:
Rastogi, D., Lehner, F., & Ashfaq, M. (2020). Revisiting recent U.S. heat waves in a warmer and more humid climate. *Geophysical Research Letters*, *47*, e2019GL086736. https://doi.org/10.1029/2019GL086736

Received 19 DEC 2019
Accepted 25 MAR 2020
Accepted article online 17 APR 2020

Revisiting Recent U.S. Heat Waves in a Warmer and More Humid Climate

Deeksha Rastogi[1,2], Flavio Lehner[3,4], and Moetasim Ashfaq[1,2]

[1]Computational Science and Engineering Division, Oak Ridge National Laboratory, Oak Ridge, TN, USA, [2]The Bredesen Center, The University of Tennessee, Knoxville, Knoxville, TN, USA, [3]National Center for Atmospheric Research, Boulder, CO, USA, [4]Institute for Atmospheric and Climate Science, ETH Zürich, Zürich, Switzerland

Abstract The frequency and intensity of heat waves in the United States is projected to increase in the 21st century. We investigate dry and humid heat waves in a pair of high-resolution model simulations that constrain large-scale atmospheric circulation, to isolate the thermodynamic impacts on characteristics of present and future heat waves over the United States. The two kinds of heat waves show differences in mean intensity, amplitude, duration, and frequency over the Southeast, Northeast, and Midwest, while their characteristics are largely similar in the drier central and western United States. In a warmer climate, relative humidity is projected to decrease during dry heat waves, whereas it remains unchanged during humid heat waves. However, the overall increase in daily maximum temperature intensifies the heat stress during future humid and dry heat waves across all regions. With large-scale circulation constrained, these simulations emphasize the importance of thermodynamic drivers in determining future heat wave characteristics.

1. Introduction

Heat waves, generally defined as persistent hot conditions above a certain threshold, severely impact socio-ecological systems by affecting human health and productivity by exerting stress on energy, agricultural yields, and ecosystems (Auffhammer et al., 2017; Bobb et al., 2014; Burke et al., 2015; Coffel et al., 2017; Lesk et al., 2016; Rastogi et al., 2019). Upward trends in the frequency, intensity, and duration of heat waves are already evident globally as well as in the United States (Cloutier-Bisbee et al., 2019; Perkins et al., 2012; Shiva et al., 2019; Smith et al., 2013; Tebaldi & Wehner, 2018). These observed changes in the characteristics of heat waves have been attributed to global warming and are projected to prevail or intensify in response to a projected increase in global temperatures (Diffenbaugh & Ashfaq, 2010; Dosio et al., 2018; Jaeger et al., 2008; Jones et al., 2018; Jones et al., 2015; King et al., 2018; Schoetter et al., 2015). The presence of high humidity levels during heat waves can further exacerbate physiological heat stress and pose severe risks to human health (Fischer & Knutti, 2013; Glaser et al., 2016) by reducing the human body's ability for evaporative cooling and by limiting heat tolerance (Dunne et al., 2013; Sherwood & Huber, 2010).

Heat wave characteristics are defined by a combination of dynamic (i.e., atmospheric circulations) and thermodynamic factors (e.g., moisture and heat fluxes). Heat waves are often associated with summertime high-pressure systems and blocking patterns. The buildup and entrainment of dry and hot air can cause dry heat waves, while the advection of hot and humid air from nearby water bodies can result in more humid heat waves. The thermodynamic characteristics of heat waves depend on land-atmosphere interactions as land surface processes play an important role in amplifying or dampening a heat wave by influencing the partitioning of available energy between sensible and latent heat fluxes (Fischer et al., 2007; Miralles et al., 2014; Raghavendra et al., 2019; Russo et al., 2017). When soil moisture is abundant, higher evaporation results in conversion of more energy to latent heat, reducing sensible heat and therefore limiting air temperature rise. Conversely, under limited soil moisture conditions, more energy is partitioned toward sensible heat, causing warm and dry conditions (Cheng et al., 2019; Lee et al., 2016; Lorenz et al., 2010; Ukkola et al., 2018). The projected increase in radiative forcing may result in enhanced surface drying and an increase in atmospheric moisture following the Clausius-Clapeyron relationship (Donat et al., 2017; Lee et al., 2016). Further, changing frequency and intensity of precipitation events are expected to increase the length of dry intervals between heavier precipitation events; this could limit soil moisture recharge and reduce evaporative cooling in a warming climate (Dai et al., 2017; Pendergrass & Knutti, 2018). Such changes in the thermodynamic characteristics have the potential to alter the character of future heat waves.

There is ample evidence regarding the influence of land-atmospheric interactions on the temperature amplification during heat waves (Lee et al., 2016; Teuling et al., 2010). For instance, reduced evaporative cooling as a result of soil moisture depletion enhanced the intensity and duration of record-breaking European heat waves (Lorenz et al., 2010; Teuling et al., 2010). Similarly, soil moisture availability has been known to influence the relationship between latent-sensible heat flux partitioning and heat wave frequency over the central United States (Lee et al., 2016). Likewise, Cheng et al. (2019) demonstrated a strong soil moisture-temperature coupling in relatively dry regions of the south-southwestern United States that intensifies in a warmer climate, whereas the moisture-abundant regions of the north-northeastern United States show a weaker coupling that also remains largely unchanged in a warmer climate. Overall, these studies highlight the importance of land-atmosphere interactions during heat waves and associated changes with warming.

Following the Clausius-Clapeyron relationship, the near-surface specific humidity is projected to rise globally with an increase in air temperature. Regionally, changes in relative humidity (RH) are more uncertain (Byrne & O'gorman, 2016; Sherwood et al., 2010). Several studies have examined the role of humidity during heat waves using heat stress indices (Coffel et al., 2019; Fischer & Knutti, 2013; Raymond et al., 2017; Russo et al., 2017; Sherwood, 2018): Raymond et al. (2017) found that wet-bulb temperature (WBT) extremes coincide more frequently with specific humidity extremes than with temperature extremes over the eastern and parts of western United States during the 1981–2015 period. Dahl et al. (2019) and Russo et al. (2017) projected an increase in the maximum apparent temperature (AT_{max}) and an enhanced human exposure to extreme heat events by the end of the 21st century. Coffel et al. (2019) showed that the effect of warming on WBT extremes can be counteracted by an enhanced drying on that day, resulting in a relative dampening of extreme WBT globally. However, the commonly used heat stress indices such as WBT or apparent temperature often include nonlinear relationships between temperature and RH and are amplified by an increase in temperature even when RH remains unchanged. Therefore, use of such indices limit our ability to isolate the role of humidity during a heat wave.

Most previous studies discussed above are based on general circulation models (GCMs) from the 5th phase of the Coupled Model Intercomparison Project (CMIP5) that conducted simulations at a relatively coarse resolution and do not resolve all local-scale processes and feedbacks (Ashfaq et al., 2016). Moreover, synoptic conditions, which are important for the occurrence of heat waves (e.g., blocking), are often not well represented in GCMs (Rasmijn et al., 2018). Finally, the simultaneous changes in dynamic and thermodynamic processes in fully coupled GCMs limit our ability to disentangle factors that drive future changes in heat wave characteristics and therefore complicate the process-based attribution of projected changes in heat waves (Wehrli et al., 2018).

Here we attempt to overcome some of the methodological and modeling limitations in earlier studies, specifically the simulation of synoptic conditions during heat waves, the identification of dominant factors that drive future changes in heat waves, and the isolation of the role of humidity during the heat waves. We use a pair of high-resolution numerical model simulations (Liu et al., 2017) and a methodology that enables the isolation of moisture-related impacts on heat waves. The large-scale atmospheric circulation in the simulations is spectrally nudged toward reanalysis data under both present-day and future climate boundary conditions. This makes the synoptic scale in the simulations reflective of the reanalysis forcing, allowing for a more realistic representation of the atmospheric conditions suitable for the occurrence of heat waves. Further, this setup keeps large-scale circulation similar in the two experiments, resulting in reoccurrence of present-day real-world atmospheric events (e.g., historic heat waves) in a future warmer climate, and enables isolation of thermodynamically driven changes in the characteristic of the heat waves.

2. Materials and Methods

2.1. Model Simulations

We use a pair of 13 year simulations conducted with the Weather Research Forecasting (WRF) model Version 3.4.1 (Skamarock et al., 2008) over a domain covering the contiguous United States and parts of Canada and Mexico detailed in Liu et al. (2017). In brief, each model simulation is conducted at a 4 km horizontal grid spacing (1,360 × 1,016 longitude-latitude grid points) with 51 vertical levels and extends from 1 October 2000 to 30 September 2013. The control simulation (WRF-CTRL) is driven by 6-hourly 0.7°

ERA-Interim data (Dee et al., 2011). The climate change experiment follows the pseudo global warming (PGW) approach (WRF-PGW), which is driven by modified ERA-Interim boundary forcing that includes a climate perturbation based on the climate change signal (2071 to 2100 minus 1976 to 2005) from the mean of 19 CMIP5 models under the Representative Concentration Pathway 8.5. The perturbation is applied to horizontal wind fields, geopotential, temperature, specific humidity, sea surface temperature, sea level pressure, sea ice, and soil temperature, but not soil moisture. Overall, the dominant climate change signal is a general warming and moistening of the atmosphere, whereas circulation changes are minimal. Within the domain, these simulations use spectral nudging toward ERA-Interim for the scales on the order of 2,000 km and greater, reproducing present-day specific synoptic weather events in both the control and perturbed simulations (supporting information Figure S1) (Liu et al., 2017). Thus, the simulations highlight future thermodynamically driven changes.

These simulations were previously used by Raghavendra et al. (2019) to evaluate heat waves over Florida. Here, we use these simulations to evaluate heat wave characteristics over the conterminous United States. We use daily maximum temperature (T_{max}), mean specific humidity, soil moisture, 850 hPa geopotential heights, and sensible and latent heat flux from these simulations. Further, we calculate evaporative fraction (EF) as the ratio of latent heat flux to total heat flux (latent + sensible) to depict energy partitioning between the two heat fluxes. The use of EF in the analyses is motivated by the reasoning that if amplified or damped warming during future heat waves is related to energy partitioning, changes in T_{max} should correlate with changes in EF during the heat waves (Donat et al., 2017).

2.2. Observational Data Set

We obtain daily T_{max} and dew point temperature (T_d) from the Parameter-Elevation Regressions on Independent Slopes Model (PRISM) (Daly et al., 2008) observational product (henceforth "observations"), available at 4 km horizontal resolution over the continental United States, for comparison during the 2001 to 2013 period.

2.3. Heat Stress Index

We use AT_{max}, also referred to as the heat index or the "feels like" temperature for the human body (Steadman, 1979), to account for the role of humidity and as a measure of heat stress during heat waves. Acknowledging that the choice of heat stress index might depend on a specific application (Buzan & Huber, 2020), we select AT_{max} over other heat stress indices, such as WBT, wet-bulb global temperature (WBGT), or T_d, for two primary reasons: (1) Differences between AT_{max} and T_{max} can be directly used to understand the role of humidity during heat waves (Russo et al., 2017) and (2) WBT and WBGT refer to heat stress when a person's skin is completely wet and unclothed or for hard exertions when a person's skin is partly wet and exposed, making them more applicable to sports and other physical activities, whereas AT_{max} more often applies to a fully clothed person who is not perspiring much (Sherwood, 2018). Overall, different heat stress metrics can yield different absolute results, but the conclusions on the role of humidity in future heat waves are robust to the choice of metric.

Here, AT_{max} is calculated by applying the Heat Index equation used by the National Oceanic and Atmospheric Administration (supporting information). We substitute AT_{max} below T_{max} with T_{max} values to focus on the amplifying effect of humidity on heat stress (Russo et al., 2017). Large differences between AT_{max} and T_{max} magnitudes during a heat wave indicate humidity as a driving factor of heat stress amplification.

2.4. Compound Heat Wave Definition

There are several ways to define heat waves, generally based on intensity and duration of high-temperature events. A widely used definition involves use of minimum number of consecutive days when temperature is above a certain threshold, absolute or percentile based (Baldwin et al., 2019; Cloutier-Bisbee et al., 2019; Horton et al., 2016; Sillmann et al., 2013). However, heat waves may often continue after a break of a day; therefore, use of the consecutive days criteria may underestimate the actual length of a heat wave. Therefore, following Baldwin et al. (2019), we use a compound heat wave definition that allows for break days: a period during summer season (June-July-August, JJA) is considered a heat wave if at least three consecutive days cross a given threshold and the heat wave continues if no more than one consecutive day falls

below the threshold. We use grid cell-based 95th percentiles of T_{max} (T_{95}) and AT_{max} (AT_{95}) as thresholds, which are based on all days of the 13 summer seasons. We calculate separate thresholds for WRF-CTRL and WRF-PGW simulations. Heat waves in WRF-CTRL are identified using only WRF-CTRL thresholds (hereafter $CTRL_{CTRL}$), while heat waves in WRF-PGW are identified using both WRF-CTRL thresholds (hereafter PGW_{CTRL}) and WRF-PGW thresholds (hereafter PGW_{PGW}). The use of two separate thresholds to find heat waves enables comparing the characteristics of heat waves (1) occurring in a warmer climate with respect to the present climate threshold (PGW_{CTRL}), (2) occurring in the present climate with respect to the present climate threshold ($CTRL_{CTRL}$), and (3) occurring in the future climate with respect to the future climate threshold (PGW_{PGW}). Together with the synoptic reoccurrence of present-day heat waves, (2) and (3) allow for a direct comparison between present and future heat waves with the mean background warming accounted for (i.e., $CTRL_{CTRL}$ and PGW_{PGW}). We apply the heat wave definition on T_{max} and AT_{max} using T_{95} and AT_{95} thresholds to identify "T_{max} heat waves" and "AT_{max} heat waves," respectively, for $CTRL_{CTRL}$, PGW_{PGW}, and PGW_{CTRL}.

2.5. Regional Analysis

We focus our analysis on four regions covering the conterminous United States: southeast, northeast-Midwest, central, and West (Figure 1m). The regions are derived from U.S. Geological Survey (USGS) climate adaptation science center regions. For ease of presentation, we combine the northwest and southwest regions as West and the north-central and south-central regions as central.

2.6. Heat Wave Indices

We use the following indices to calculate heat wave characteristics:

1. Duration of heat wave: number of days above the threshold including the break days
2. Mean amplitude: average of T_{max} over the length of heat wave excluding the break days
3. Mean heat wave intensity: average difference between T_{max} and T_{95} over the length of heat wave excluding the break days
4. Number of heat waves: total count of heat waves that occur during summer
5. Percentage area under heat wave: fraction of the total grid points (in percent) in a region that is under a heat wave on a given day

3. Results

3.1. Characteristics of T_{max} Versus AT_{max} Heat Waves

We first evaluate the characteristics (duration, intensity, and area) of T_{max} and AT_{max} heat waves (Figure 1) that occurred in observations during the analyses period (2001 to 2013) over the four geographical regions (Figure 1m). The southeast, which is the most humid region in the United States, generally shows a higher mean percentage area and mean intensity for AT_{max} heat waves as compared to T_{max} heat waves with the exception of a few years (Figures 1d and 1h). We illustrate this point by showing a comparison for summer 2010, when a higher percentage of the southeast was under AT_{max} heat wave when compared to T_{max} heat wave (Figure 1i). This shows that humidity can affect, and in this case exacerbate, the geographical footprint of heat waves. The impact of humidity is further evident from the large differences between AT_{max} and T_{max} in the southeast during the 2010 heat waves, suggesting that humidity amplified those heat waves (Figures 1k and 1l). Contrarily, summer 2012 was relatively dry in the southeast, with a higher percentage of area under T_{max} heat waves compared to that under AT_{max} heat waves and comparatively smaller differences between AT_{max} and T_{max} during heat waves (Figures 1j, 1m, and 1n).

The northeast-midwestern United States displays mixed behavior with generally higher mean intensity values for AT_{max} as compared to T_{max} heat waves, whereas the mean percentage area is similar under AT_{max} and T_{max} heat waves (Figures 1c and 1g). On the other hand, the central and West (Figures 1a, 1b, 1e, and 1f) generally exhibit indistinguishable characteristics for the two kinds of heat waves, consistent with the predominantly dry summer in these regions. Overall, heat waves last for up to 8 days, with the majority lasting between 3 and 6 days across the four regions for both T_{max} and AT_{max} (Figures 1a–1h).

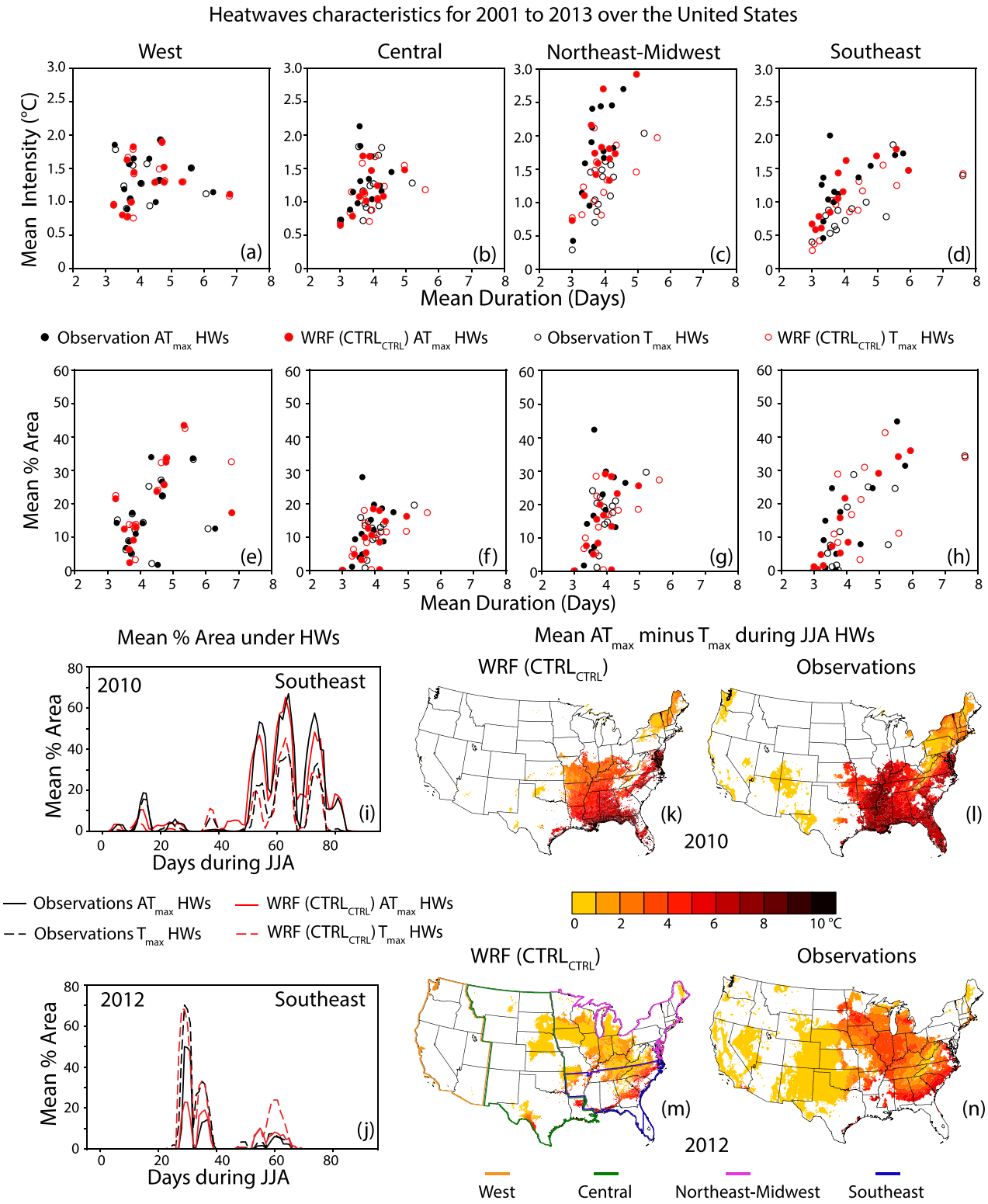

Figure 1. (a–h) Scatter plots of mean duration versus (a–d) mean intensity and (e–h) mean percentage area for the heat waves over West, Central, Northeast-Midwest, and Southeast United States, respectively. The four regions are marked in 1 m. Circles (filled for AT_{max} and hollow for T_{max}; black for PRISM [observations] and red for WRF $CTRL_{CTRL}$) represent averages during heat waves for each summer (JJA). Lines (solid for AT_{max} and dashed for T_{max}; black for observations and red for WRF $CTRL_{CTRL}$) show mean percentage area under heat waves over the Southeast for JJA during (i) 2010 and (j) 2012. (k–n) Spatial maps show average differences between AT_{max} and T_{max} during the heat wave days in 2010 for (k) WRF ($CTRL_{CTRL}$) and (l) observations and in 2012 for (m) WRF ($CTRL_{CTRL}$) and (n) observations.

3.2. WRF-CTRL Versus Observations

We compare the simulated (WRF-CTRL) and observed (PRISM) characteristics of both T_{max} and AT_{max} heat waves for the analyses period (Figures 1a–1h, S2, and S3). Overall, WRF-CTRL simulates a comparable range for both mean intensity (Figures 1a–1d) and mean percentage area (Figures 1e–1f) over the four regions. The spatial patterns of characteristics such as length, total number of heat waves, amplitude, intensity of T_{max} and AT_{max} heat waves, and T_{95} and AT_{95}, compare well with the observed characteristics, with the exception of a few noticeable biases in their magnitudes (Figures S2 and S3). For instance, WRF-CTRL underestimates the frequency of T_{max} and AT_{max} heat waves in the West and AT_{max} heat waves in the southeast and parts of the Midwest. WRF-CTRL also exhibits positive biases in simulating the amplitudes of both T_{max} and AT_{max} heat waves and T_{95} and AT_{95}, primarily over the central and southeast (Figures S2 and S3). These biases in the magnitude of heat waves are possibly associated with the prevailing warm season (May to October) biases in these simulations (Liu et al., 2017). A near-surface temperature warm bias of up to 3 °C exists in the central and cold biases of up to 2 °C in the southeast and Midwest and up to 1 °C bias in the northeast during summer (Liu et al., 2017), which are partly attributed to mean biases in simulated soil moisture in these regions (Figure S4).

To revisit the specific cases discussed before, during 2010, WRF-CTRL reproduces the observed percentage area under T_{max} and AT_{max} heat waves (Figure 1i). The spatial pattern of where AT_{max} is larger than T_{max} is simulated well. WRF-CTRL slightly underestimates the amplification of AT_{max} relative to T_{max} along the Lower Mississippi (Figures 1k and 1l). During 2012, WRF-CTRL exhibits some biases, underestimating the area where AT_{max} exceeds T_{max} (Figures 1j, 1m, and 1n). Overall, WRF-CTRL is able to capture the spatiotemporal characteristics of observed heat waves during 2001–2013 reasonably well.

3.3. Changes in the Characteristics of Heat Waves in a Warmer Climate

Changes in moisture availability during heat waves can influence their characteristics. To investigate such influences, we plot RH against T_{max} during both T_{max} and AT_{max} heat waves in observations, $CTRL_{CTRL}$, PGW_{CTRL}, and PGW_{PGW} (Figure 2). Due to strong warming, more than half of the summer days over the majority of the United States qualify as part of a heat wave in the future climate (Figure S5). Therefore, future heat waves defined using the CTRL threshold (PGW_{CTRL}) are more representative of the future average summer conditions rather than heat wave conditions (e.g., Lehner et al., 2016). As a result, a significant increase in the duration and frequency of heat waves is projected in PGW_{CTRL} (Figure S6). RH during T_{max} heat waves shows only small differences between PGW_{CTRL} and $CTRL_{CTRL}$. Contrarily, PGW_{PGW}, which represents future heat waves defined relative to the future climate, shows T_{max} increasing by an average of at least 5 °C in all regions compared to $CTRL_{CTRL}$ (Figure 2). RH during T_{max} heat waves in PGW_{PGW} is projected to decrease in all regions except the West where it is historically low already. The strongest decrease occurs in the southeast and northeast-Midwest (Figures 2a–2d). Specific humidity, in turn, does not change much during future T_{max} heat waves (Figure S7). Conversely, during future AT_{max} heat waves, which by definition tend to be more humid than T_{max} heat waves, RH remains largely unchanged due to increases in both specific humidity and T_{max} in PGW_{PGW} and PGW_{CTRL} (Figures 2 and S7). Together, these simulated changes suggest that temperature-defined heat waves become drier in the future, whereas humid heat waves maintain their character (Figures 2e–2h).

Given the use of spectral nudging in these simulations, CTRL heat waves are likely to reappear in a similar but not identical fashion in PGW (Figure S1), allowing for a direct comparison between PGW_{PGW} and $CTRL_{CTRL}$ heat wave characteristics (Figure S5). This close correspondence is confirmed by the fact that heat wave metrics such as duration, area, and frequency, which are largely controlled by the synoptic conditions, are very similar between $CTRL_{CTRL}$ and PGW_{PGW} on a seasonal basis, while subtle differences can occur for individual heat waves (not shown). Using paired differences between PGW_{PGW} and $CTRL_{CTRL}$ heat waves for 13 summer seasons, we aim to identify differences that are robust to these methodological uncertainties. We generally find higher intensities of T_{max} heat waves that are significant (95% confidence level) over the central and West, and higher intensities of AT_{max} heat waves that are significant over all regions (Figure S8).

To better understand the mechanisms driving these differences in intensity, we analyze thermodynamic changes in the characteristics of heat waves. For T_{max} heat waves in PGW_{CTRL}, which span more than half of future summer days over the majority of the United States (Figure S5), the latent and sensible heating

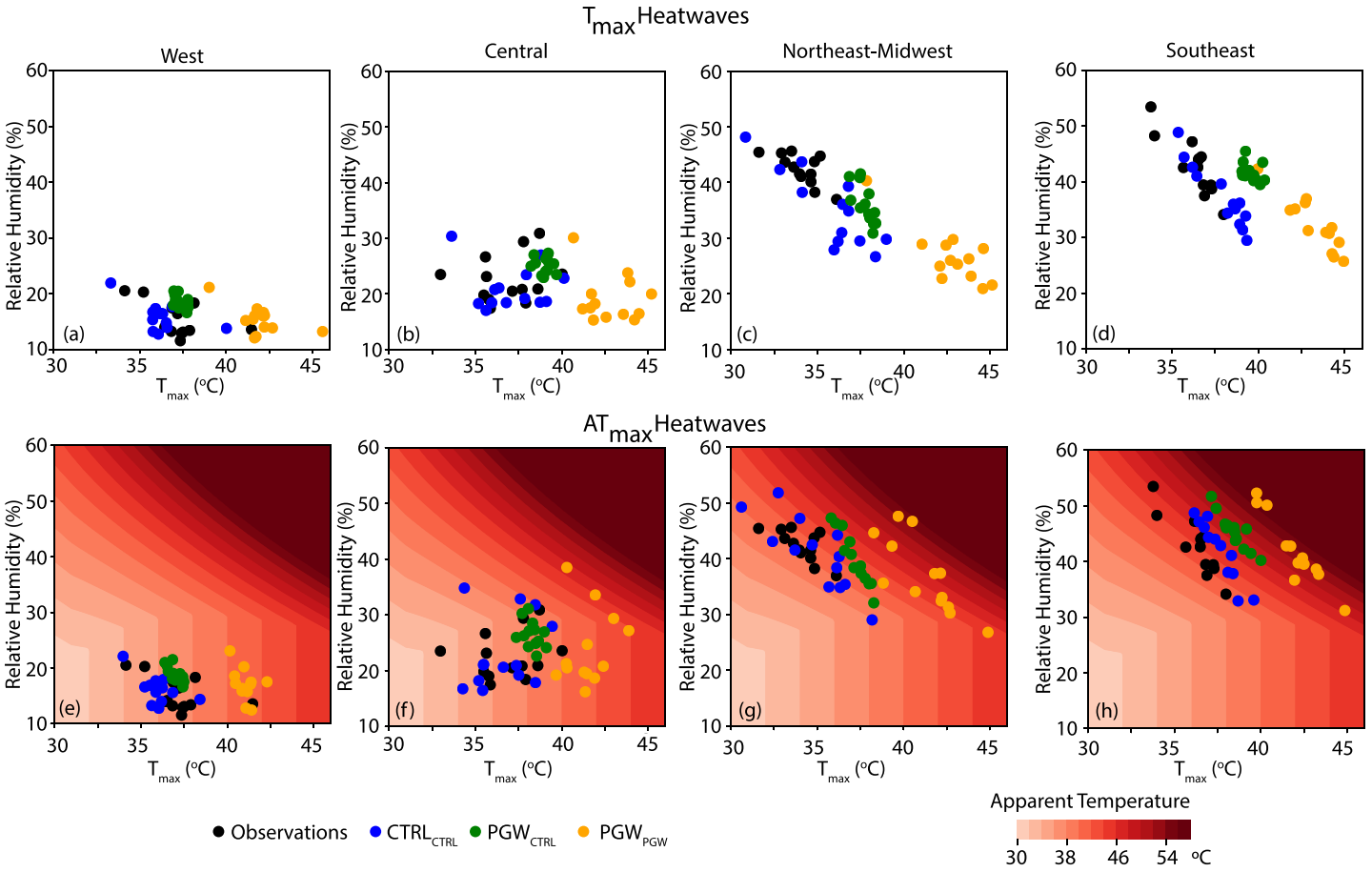

Figure 2. Scatter plots between T_{max} versus RH during (a–d) T_{max} heat waves and (e–h) AT_{max} heat waves for four regions. Black, blue, green, and yellow circles represent the averages across heat waves occurring during each summer in observations, CTRL simulations with respect to the CTRL threshold ($CTRL_{CTRL}$), PGW simulations with respect to the CTRL threshold (PGW_{CTRL}), and PGW simulations with respect to the PGW threshold (PGW_{PGW}), respectively. Background contours in (e) to (h) correspond to respective AT_{max} values.

exhibit only minor changes with respect to $CTRL_{CTRL}$ over all regions with the exception of small but significant increases in latent heating over the southeast and sensible heating over the northeast-Midwest (green boxes in Figures 3a and 3b). Conversely, for T_{max} heat waves in PGW_{PGW} (red boxes in Figures 3a and 3b), latent heat and sensible heat fluxes show significant changes in all regions. Generally, dry regions (West and central) see smaller changes in heat fluxes than more humid regions (northeast-Midwest and southeast), with the latter showing a clear increase in the partitioning of energy toward sensible heat. This corroborates the results in Figure 2, which suggest future summers will experience constant or increased RH, but future heat waves will see decreases in RH, particularly in humid regions, thus relatively damping future heat stress on the hottest days (Coffel et al., 2019). Further, changes in heat fluxes, especially during PGW_{PGW} T_{max} heat waves, closely correspond to changes in soil moisture, with projected decreases in latent heat flux and increases in sensible heat flux generally being associated with decreases in soil moisture during heat waves (Figure S9a).

During AT_{max} heat waves, heat fluxes exhibit only small changes (Figures 3c and 3d), which also approximately correspond to changes in soil moisture being generally small and insignificant over most regions with the exception of stronger soil moisture decreases over the northeast-Midwest (Figure S9b). Specifically, PGW_{CTRL} (green boxes in Figures 3c and 3d) shows a mixed response for latent heat fluxes with no mean change in the West, small but significant increases in the central and southeast, and small decreases in the northeast-Midwest. Likewise, sensible heat fluxes in PGW_{CTRL} show negligible changes in all regions with the exception of significant increases in the northeast-Midwest. Contrarily, PGW_{PGW} (red boxes in

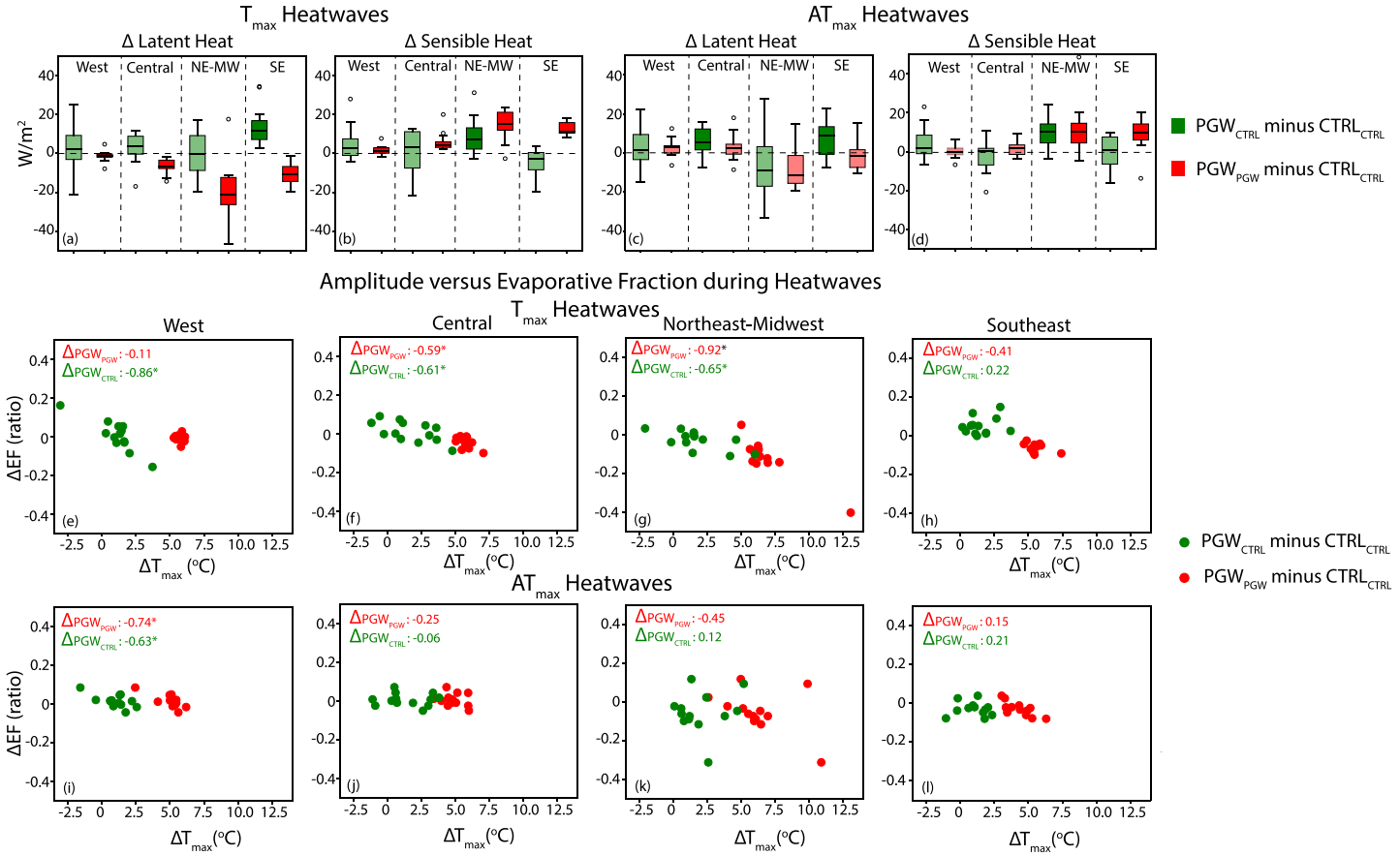

Figure 3. Box and whisker plots (a to d) show spread in paired differences in heat fluxes between corresponding present and future summers during T_{max}, AT_{max} heat waves for (a, c) latent heat and (b, d) sensible heat fluxes. Darker shading inside the box shows significance at 95% confidence level using two-sided Student's *T* test, whereas lighter shading is used where the change is not significant. Green and red boxes represent the change between PGW_{CTRL} and $CTRL_{CTRL}$ and between PGW_{PGW} and $CTRL_{CTRL}$ heat waves, respectively. In the box and whisker plots, the center line shows the 50th percentile, the bottom and top boundaries of the box indicate first (Q1) and third (Q3) quartiles, respectively; the whiskers extend 1.5 times the interquartile length (Q3–Q1) beyond the box boundaries. The hollow circles are the outliers. Scatter plots (e–l) between changes in T_{max} versus changes in evaporative fraction (EF) for (e–h) T_{max} and (i–l) AT_{max} heat waves for four regions. Green and red boxes circles represent the change between PGW_{CTRL} and $CTRL_{CTRL}$ and between PGW_{PGW} and $CTRL_{CTRL}$ heat waves, respectively. Numbers in e–l show correlation coefficients between the changes, and color of the statistics correspond to the respective scatter. The significant statistics at 95% confidence level are marked with asterisks.

Figures 3c and 3d) exhibits negligible changes in heat fluxes over both the West and central and insignificant decreases in latent heat fluxes and significant increase in sensible heat fluxes over both the northeast-Midwest and southeast.

To further establish the role of land-atmosphere interactions in driving variations in the characteristics of heat waves, we investigate the relationship between changes in EF and changes in T_{max} during future heat waves (Figures 3e–3l). During T_{max} heat waves, changes in EF are significantly negatively correlated with changes in T_{max} over most regions except the southeast, consistent with the idea that in regions where moisture is not abundant, moisture limitation can amplify or dampen temperature anomalies via EF (Figures 3e–3h). These relationships occur over all regions in both PGW_{CTRL} and PGW_{PGW}, except in the West where it does not occur in PGW_{PGW} and the southeast where it does not occur in PGW_{CTRL} heat waves. In turn, for AT_{max} heat waves, where moisture is typically abundant, correlations between EF and T_{max} are insignificant everywhere, except for the West (Figures 3i–3l). Overall, these changes are in line with the expectation that the amplified warming during T_{max} heat waves is closely associated with reduced evaporative cooling, portraying land-atmosphere interactions as the primary driver of the amplification of T_{max} heat waves. Conversely, a weak relationship between the changes in EF and changes in T_{max} during AT_{max} heat waves indicates a weak land-atmosphere coupling during more humid heat waves in both present and future climates.

4. Conclusion and Discussion

Using a set of high-resolution spectrally nudged WRF model simulations, we evaluate changes in the characteristics of temperature-based and temperature-humidity-based heat waves (T_{max} and AT_{max}) in a warmer climate. We find a decrease in RH during future T_{max} heat waves and no significant change in RH during future AT_{max} heat waves with reference to the control period. Given that AT_{max} depends on both RH and T_{max}, higher T_{max} during humid heat waves drives an increase in AT_{max}, even if RH remains largely unchanged. Changes in T_{max} during T_{max} heat waves are correlated with changes in EF, which reflects a stronger land-atmosphere coupling during these heat waves. Contrarily, generally weak or no relationship exists between the changes in EF and T_{max} during AT_{max} heat waves, indicating a weak role of land-atmosphere coupling in the future changes of AT_{max} heat waves. Overall, higher temperatures in a warmer climate can result in reduced soil moisture during the warm season, causing an increase in the sensible heat flux and a decrease in the latent heat flux. These relationships are well visible during T_{max} heat waves.

The findings associated with T_{max} heat waves are generally consistent with previous studies, which associate intensification of temperature extremes with higher partitioning to sensible heat as a result of stronger land-atmosphere coupling under moisture-limited circumstances (Coffel et al., 2019; Donat et al., 2018, 2017; Fischer & Knutti, 2013; Lee et al., 2016; Teuling et al., 2010). In more moisture-abundant circumstances, such as described by AT_{max} heat waves, the lack of substantial changes in the energy flux partitioning yields no amplification of heat wave characteristics beyond the mean warming. This is consistent with previously reported undetectable changes in the land-atmosphere interactions in moisture-abundant regions over the United States (Cheng et al., 2019).

Overall, this study provides a new but complementary perspective on the changing characteristics of heat waves in a future climate. The design of our experiments, with large-scale atmospheric circulation spectrally nudged, allows us to more robustly associate these changes to thermodynamic processes. However, future heat waves are still likely to be affected by changes in the atmospheric circulation, although these are typically less robust across models (Barnes et al., 2014; Gibson et al., 2017; Sussman et al., 2020). The results here suggest that circulation changes are unlikely to be a dominant factor needed to explain changing heat wave characteristics. This is consistent with results from fully coupled GCMs, but a comprehensive assessment of changes in the heat waves and heat stress hazard nonetheless needs to account for both dynamic and thermodynamic factors. An analysis of large ensembles of fully coupled simulations is needed to understand the contribution from different drivers at the regional scale and to overcome limitations of this study with regard to sample size and thus statistical significance. Here we identify the role of humidity during heat waves using one heat stress index, but further exploration using other available heat stress indices might be useful since different indices show varying sensitivity to humidity.

Acknowledgments
This study is partly supported by the Energy Exascale Earth System Model (E3SM), funded by the U.S. Department of Energy (DOE), Office of Science, Office of Biological and Environmental Research (BER) and by Advance Study Program fellowship awarded by Graduate Visitor Program at National Center for Atmospheric Research (NCAR). F. L. is supported by NSF AGS-0856145, Amendment 87 and the Regional and Global Model Analysis (RGMA) component of the Earth and Environmental System Modeling Program of the U.S. DOE's Office of BER via NSF IA 1947282. Support for data storage and analysis is provided by Computational Information Systems Laboratory at NCAR. Data used in this study can be accessed by contacting the lead authors of Liu et al. (2017). This manuscript has been authored by employees of UT-Battelle, LLC, under Contract DEAC05-00OR22725 with the U.S. Department of Energy (DOE). Accordingly, the publisher, by accepting the article for publication, acknowledges that the U.S. government retains a nonexclusive, paid-up, irrevocable, worldwide license to publish or reproduce the published form of this manuscript, or allow others to do so, for U.S. government purposes. DOE will provide public access to these results of federally sponsored research in accordance with the DOE Public Access Plan (http://energy.gov/downloads/doepublicaccess-plan).

References

Ashfaq, M., Rastogi, D., Mei, R., Kao, S. C., Gangrade, S., Naz, B. S., & Touma, D. (2016). High-resolution ensemble projections of near-term regional climate over the continental United States. *Journal of Geophysical Research: Atmospheres*, *121*, 9943–9963. https://doi.org/10.1002/2016JD025285

Auffhammer, M., Baylis, P., & Hausman, C. H. (2017). Climate change is projected to have severe impacts on the frequency and intensity of peak electricity demand across the United States. *Proceedings of the National Academy of Sciences*, *114*(8), 1886–1891. https://doi.org/10.1073/pnas.1613193114

Baldwin, J. W., Dessy, J. B., Vecchi, G. A., & Oppenheimer, M. (2019). Temporally compound heat wave events and global warming: An emerging hazard. *Earth's Future*, *7*(4), 411–427. https://doi.org/10.1029/2018ef000989

Barnes, E. A., Dunn-Sigouin, E., Masato, G., & Woollings, T. (2014). Exploring recent trends in Northern Hemisphere blocking. *Geophysical Research Letters*, *41*(2), 638–644. https://doi.org/10.1002/2013GL058745

Bobb, J. F., Peng, R. D., Bell, M. L., & Dominici, F. (2014). Heat-related mortality and adaptation to heat in the United States. *Environmental Health Perspectives*, *122*(8), 811–816. https://doi.org/10.1289/ehp.1307392

Burke, M., Hsiang, S. M., & Miguel, E. (2015). Global non-linear effect of temperature on economic production. *Nature*, *527*(7577), 235–239. https://doi.org/10.1038/nature15725

Buzan, J. R., & Huber, M. (2020). Moist heat stress on a hotter Earth. *Annual Review of Earth and Planetary Sciences*, *48*(1). https://doi.org/10.1146/annurev-earth-053018-060100

Byrne, M. P., & O'gorman, P. A. (2016). Understanding decreases in land relative humidity with global warming: Conceptual model and GCM simulations. *Journal of Climate*, *29*(24), 9045–9061. https://doi.org/10.1175/JCLI-D-16-0351.1

Cheng, L., Hoerling, M., Liu, Z., & Eischeid, J. (2019). Physical understanding of human-induced changes in US hot droughts using equilibrium climate simulations. *Journal of Climate*, *32*(14), 4431–4443. https://doi.org/10.1175/JCLI-D-18-0611.1

Cloutier-Bisbee, S. R., Raghavendra, A., & Milrad, S. M. (2019). Heat waves in Florida: Climatology, trends, and related precipitation events. *Journal of Applied Meteorology and Climatology*, *58*(3), 447–466. https://doi.org/10.1175/JAMC-D-18-0165.1

Coffel, E. D., Horton, R. M., Winter, J. M., & Mankin, J. S. (2019). Nonlinear increases in extreme temperatures paradoxically dampen increases in extreme humid-heat. *Environmental Research Letters*, *14*(8). https://doi.org/10.1088/1748-9326/ab28b7

Coffel, E. D., Thompson, T. R., & Horton, R. M. (2017). The impacts of rising temperatures on aircraft takeoff performance. *Climatic Change*, *144*(2), 381–388. https://doi.org/10.1007/s10584-017-2018-9

Dahl, K., Licker, R., Abatzoglou, J. T., & Declet-Barreto, J. (2019). Increased frequency of and population exposure to extreme heat index days in the United States during the 21st century. *Environmental Research Communications*, *1*(7), 075002. https://doi.org/10.1088/2515-7620/ab27cf

Dai, A., Rasmussen, R. M., Liu, C., Ikeda, K., & Prein, A. F. (2017). A new mechanism for warm-season precipitation response to global warming based on convection-permitting simulations. *Climate Dynamics*, 1–26. https://doi.org/10.1007/s00382-017-3787-6

Daly, C., Halbleib, M., Smith, J. I., Gibson, W. P., Doggett, M. K., Taylor, G. H., et al. (2008). Physiographically sensitive mapping of climatological temperature and precipitation across the conterminous United States. *International Journal of Climatology*, *28*(15), 2031–2064. https://doi.org/10.1002/joc.1688

Dee, D. P., Uppala, S. M., Simmons, A. J., Berrisford, P., Poli, P., Kobayashi, S., et al. (2011). The ERA-Interim reanalysis: Configuration and performance of the data assimilation system. *Quarterly Journal of the Royal Meteorological Society*, *137*(656), 553–597. https://doi.org/10.1002/qj.828

Diffenbaugh, N. S., & Ashfaq, M. (2010). Intensification of hot extremes in the United States. *Geophysical Research Letters*, *37*, L15701. https://doi.org/10.1029/2010GL043888

Donat, M. G., Pitman, A. J., & Angélil, O. (2018). Understanding and reducing future uncertainty in Midlatitude daily heat extremes via land surface feedback constraints. *Geophysical Research Letters*, *45*(19), 10,627–610,636. https://doi.org/10.1029/2018GL079128

Donat, M. G., Pitman, A. J., & Seneviratne, S. I. (2017). Regional warming of hot extremes accelerated by surface energy fluxes. *Geophysical Research Letters*, *44*(13), 7011–7019. https://doi.org/10.1002/2017gl073733

Dosio, A., Mentaschi, L., Fischer, E. M., & Wyser, K. (2018). Extreme heat waves under 1.5 °C and 2 °C global warming. *Environmental Research Letters*, *13*(5), 054006. https://doi.org/10.1088/1748-9326/aab827

Dunne, J. P., Stouffer, R. J., & John, J. G. (2013). Reductions in labour capacity from heat stress under climate warming. *Nature Climate Change*, *3*(6), 563–566. https://doi.org/10.1038/Nclimate1827

Fischer, E. M., & Knutti, R. (2013). Robust projections of combined humidity and temperature extremes. *Nature Climate Change*, *3*(2), 126–130. https://doi.org/10.1038/Nclimate1682

Fischer, E. M., Seneviratne, S. I., Vidale, P. L., Luthi, D., & Schar, C. (2007). Soil moisture-atmosphere interactions during the 2003 European summer heat wave. *Journal of Climate*, *20*(20), 5081–5099. https://doi.org/10.1175/Jcli4288.1

Gibson, P. B., Pitman, A. J., Lorenz, R., & Perkins-Kirkpatrick, S. E. (2017). The role of circulation and land surface conditions in current and future Australian heat waves. *Journal of Climate*, *30*(24), 9933–9948. https://doi.org/10.1175/JCLI-D-17-0265.1

Glaser, J., Lemery, J., Rajagopalan, B., Diaz, H. F., García-Trabanino, R., Taduri, G., et al. (2016). Climate change and the emergent epidemic of CKD from heat stress in rural communities: The case for heat stress nephropathy. *Journal of the American Society of Nephrology*, *11*(8), 1472–1483. https://doi.org/10.2215/Cjn.13841215

Horton, R. M., Mankin, J. S., Lesk, C., Coffel, E., & Raymond, C. (2016). A review of recent advances in research on extreme heat events. *Current Climate Change Reports*, *2*(4), 242–259. https://doi.org/10.1007/s40641-016-0042-x

Jaeger, C. C., Krause, J., Haas, A., Klein, R., & Hasselmann, K. (2008). A method for computing the fraction of attributable risk related to climate damages. *Risk Analysis*, *28*(4), 815–823. https://doi.org/10.1111/j.1539-6924.2008.01070.x

Jones, B., O'Neill, B. C., McDaniel, L., McGinnis, S., Mearns, L. O., & Tebaldi, C. (2015). Future population exposure to US heat extremes. *Nature Climate Change*, *5*(7), 652–655. https://doi.org/10.1038/nclimate2631

Jones, B., Tebaldi, C., O'Neill, B. C., Oleson, K., & Gao, J. (2018). Avoiding population exposure to heat-related extremes: Demographic change vs climate change. *Climatic Change*, *146*(3–4), 423–437. https://doi.org/10.1007/s10584-017-2133-7

King, A. D., Donat, M. G., Lewis, S. C., Henley, B. J., Mitchell, D. M., Stott, P. A., et al. (2018). Reduced heat exposure by limiting global warming to 1.5 °C. *Nature Climate Change*, *8*(7), 549–551. https://doi.org/10.1038/s41558-018-0191-0

Lee, E., Bieda, R., Shanmugasundaram, J., & Richter, H. B. (2016). Land surface and atmospheric conditions associated with heat waves over the Chickasaw Nation in the south central United States. *Journal of Geophysical Research: Atmospheres*, *121*, 6284–6298. https://doi.org/10.1002/2015JD024659

Lehner, F., Deser, C., & Sanderson, B. M. (2016). Future risk of record-breaking summer temperatures and its mitigation. *Climatic Change*, *146*(3–4), 363–375. https://doi.org/10.1007/s10584-016-1616-2

Lesk, C., Rowhani, P., & Ramankutty, N. (2016). Influence of extreme weather disasters on global crop production. *Nature*, *529*(7584), 84–87. https://doi.org/10.1038/nature16467

Liu, C. H., Ikeda, K., Rasmussen, R., Barlage, M., Newman, A. J., Prein, A. F., et al. (2017). Continental-scale convection-permitting modeling of the current and future climate of North America. *Climate Dynamics*, *49*(1–2), 71–95. https://doi.org/10.1007/s00382-016-3327-9

Lorenz, R., Jaeger, E. B., & Seneviratne, S. I. (2010). Persistence of heat waves and its link to soil moisture memory. *Geophysical Research Letters*, *37*, L09703. https://doi.org/10.1029/2010GL042764

Miralles, D. G., Teuling, A. J., van Heerwaarden, C. C., & de Arellano, J. V. G. (2014). Mega-heatwave temperatures due to combined soil desiccation and atmospheric heat accumulation. *Nature Geoscience*, *7*(5), 345–349. https://doi.org/10.1038/Ngeo2141

Pendergrass, A. G., & Knutti, R. (2018). The uneven nature of daily precipitation and its change. *Geophysical Research Letters*, *45*, 11–980.

Perkins, S. E., Alexander, L. V., & Nairn, J. R. (2012). Increasing frequency, intensity and duration of observed global heatwaves and warm spells. *Geophysical Research Letters*, *39*, L20714. https://doi.org/10.1029/2012gl053361

Raghavendra, A., Dai, A. G., Milrad, S. M., & Cloutier-Bisbee, S. R. (2019). Floridian heatwaves and extreme precipitation: Future climate projections. *Climate Dynamics*, *52*(1–2), 495–508. https://doi.org/10.1007/s00382-018-4148-9

Rasmijn, L. M., van der Schrier, G., Bintanja, R., Barkmeijer, J., Sterl, A., & Hazeleger, W. (2018). Future equivalent of 2010 Russian heatwave intensified by weakening soil moisture constraints. *Nature Climate Change*, *8*(5), 381–385. https://doi.org/10.1038/s41558-018-0114-0

Rastogi, D., Holladay, J. S., Evans, K. J., Preston, B., & Ashfaq, M. (2019). Shift in seasonal climate patterns likely to impact residential energy consumption in the United States. *Environmental Research Letters*, *14*(7), 074006. https://doi.org/10.1088/1748-9326/ab22d2

Raymond, C., Singh, D., & Horton, R. M. (2017). Spatiotemporal patterns and synoptics of extreme wet-bulb temperature in the contiguous United States. *Journal of Geophysical Research: Atmospheres*, *122*, 13,108–13,124. https://doi.org/10.1002/2017JD027140

Russo, S., Sillmann, J., & Sterl, A. (2017). Humid heat waves at different warming levels. *Scientific Reports*, *7*(1), 1–7. https://doi.org/10.1038/s41598-017-07536-7

Schoetter, R., Cattiaux, J., & Douville, H. (2015). Changes of western European heat wave characteristics projected by the CMIP5 ensemble. *Climate Dynamics*, *45*(5–6), 1601–1616. https://doi.org/10.1007/s00382-014-2434-8

Sherwood, S. C. (2018). How important is humidity in heat stress? *Journal of Geophysical Research: Atmospheres*, *123*, 11,808–811,810. https://doi.org/10.1029/2018JD028969

Sherwood, S. C., & Huber, M. (2010). An adaptability limit to climate change due to heat stress. *Proceedings of the National Academy of Sciences*, *107*(21), 9552–9555. https://doi.org/10.1073/pnas.0913352107

Sherwood, S. C., Ingram, W., Tsushima, Y., Satoh, M., Roberts, M., Vidale, P. L., & O'Gorman, P. A. (2010). Relative humidity changes in a warmer climate. *Journal of Geophysical Research*, *115*, D09104. https://doi.org/10.1029/2009JD012585

Shiva, J. S., Chandler, D. G., & Kunkel, K. E. (2019). Localized changes in heat wave properties across the United States. *Earth's Future*, *7*(3), 300–319. https://doi.org/10.1029/2018ef001085

Sillmann, J., Kharin, V. V., Zwiers, F. W., Zhang, X., & Bronaugh, D. (2013). Climate extremes indices in the CMIP5 multimodel ensemble: Part 2. Future climate projections. *Journal of Geophysical Research: Atmospheres*, *118*, 2473–2493. https://doi.org/10.1002/jgrd.50188

Skamarock, W. C., Klemp J. B., Dudhia J., Gill D. O., Barker D. M., W. Wang, and Powers J. G. (2008), A description of the Advanced Research WRF version 3. NCAR Technical note-475+ STR.

Smith, T. T., Zaitchik, B. F., & Gohlke, J. M. (2013). Heat waves in the United States: Definitions, patterns and trends. *Climatic Change*, *118*(3–4), 811–825. https://doi.org/10.1007/s10584-012-0659-2

Steadman, R. G. (1979). Assessment of sultriness.1. Temperature-humidity index based on human physiology and clothing science. *Journal of Applied Meteorology*, *18*(7), 861–873. https://doi.org/10.1175/1520-0450(1979)018<0861:Taospi>2.0.Co;2

Sussman, H. S., Raghavendra, A., Roundy, P. E., & Dai, A. (2020). Trends in northern midlatitude atmospheric wave power from 1950 to 2099. *Climate Dynamics*, *54*, 1–16.

Tebaldi, C., & Wehner, M. F. (2018). Benefits of mitigation for future heat extremes under RCP4.5 compared to RCP8.5. *Climatic Change*, *146*(3–4), 349–361. https://doi.org/10.1007/s10584-016-1605-5

Teuling, A. J., Seneviratne, S. I., Stöckli, R., Reichstein, M., Moors, E., Ciais, P., et al. (2010). Contrasting response of European forest and grassland energy exchange to heatwaves. *Nature Geoscience*, *3*(10), 722–727. https://doi.org/10.1038/ngeo950

Ukkola, A. M., Pitman, A. J., Donat, M. G., De Kauwe, M. G., & Angelil, O. (2018). Evaluating the contribution of land-atmosphere coupling to heat extremes in CMIP5 models. *Geophysical Research Letters*, *45*(17), 9003–9012. https://doi.org/10.1029/2018GL079102

Wehrli, K., Guillod, B. P., Hauser, M., Leclair, M., & Seneviratne, S. I. (2018). Assessing the dynamic versus thermodynamic origin of climate model biases. *Geophysical Research Letters*, *45*(16), 8471–8479. https://doi.org/10.1029/2018GL079220